Supplementary Material (for publication), L. Oltedal & E. Hartveit

Terminal-end versus soma-end recordings for capacitance measurements

Our preference for terminal-end recording seems to directly contradict the work of Zhou et al. (2006) who used soma-end recordings from acutely isolated mouse rod bipolar cells to measure depolarization-evoked exocytosis occurring at the axon terminals (see also Wan et al., 2008). It is important to note, however, that Zhou et al. (2006) carefully selected rod bipolar cells with short and thick axons. To explore the consequences of these morphological properties for capacitance measurements, we constructed a simplified computer model of a mouse rod bipolar cell in NEURON (cf. Oltedal et al., 2007; Suppl. Fig. 1). The model was based on the morphological and passive membrane properties reported by Zhou et al. (2006): soma = 8 μm length and 8 μm diameter, axon = 32 μm length and 1 μm diameter, axon terminal = 6 μm length and 5 μm diameter, specific membrane capacitance = 0.9 μF cm^{-2} (resulting in a total capacitance of 3.6 pF), specific membrane resistance = 10 kΩ cm^2 (selected to give an input resistance of 2.6 GΩ), R_i = 160 Ω cm, and e_pas = -60 mV. With simulations as in Fig. 1 and a sine wave frequency of 800 Hz (used by Zhou et al., 2006), the accuracy of ΔC_m measurements for soma-end recording (0.76) was almost as high as for terminal-end recording (0.84; Suppl. Fig. 1). With the higher sine wave frequency used in our recordings (2 kHz), the accuracy of soma-end recording dropped dramatically to 0.17, while it only fell to 0.65 for terminal-end recording (Suppl. Fig. 1). These results suggest that for isolated rod bipolar cells, selected on the basis of specific morphological characteristics, soma-end recordings in combination with moderately high sine wave frequencies can be used for measuring exocytotic capacitance increases. It is doubtful, however, that the necessary morphological selection can be adequately performed in a slice preparation. This is unfortunate, because the slice preparation has

the potential to combine presynaptic capacitance measurements from rod bipolar cells with postsynaptic recordings from AII amacrine cells, in this case paired recordings from rod bipolar axon terminals and AII amacrine cells.

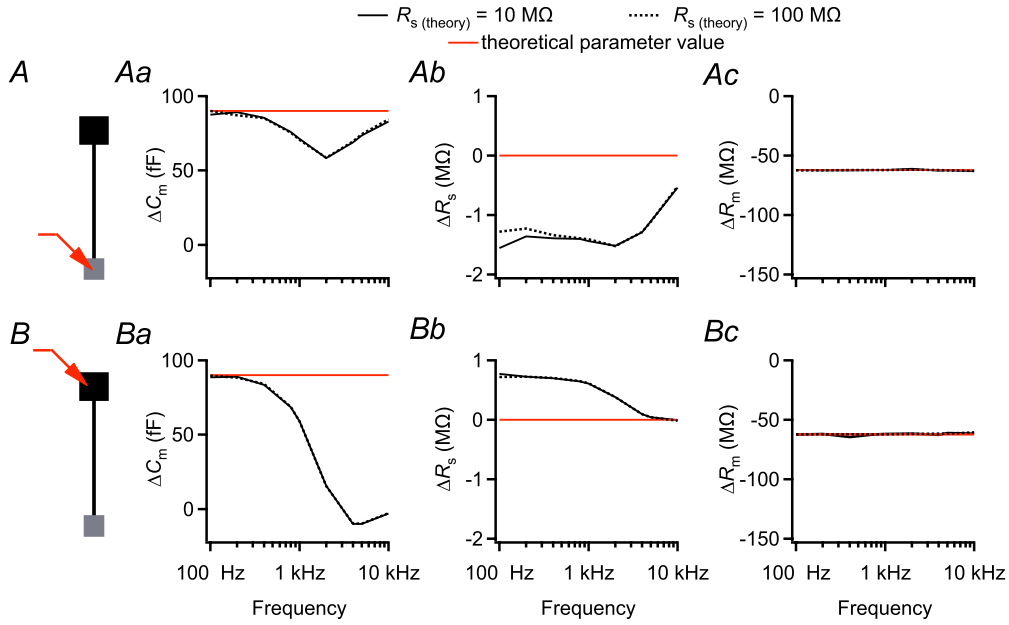

Supplementary Figure 1. Performance of the "Sine + DC" technique using computer simulations of either terminal-end (***A***) or soma-end recording (***B***) of short-axon rod bipolar cells and capacitance increase occurring at the axon terminal. ***A***, shape plot of idealized rod bipolar cell used for computer simulations. *Red* arrow indicates position of idealized single-electrode voltage clamp (SEClamp) connected to axon terminal where a capacitance increase was simulated (*gray*). ***Aa-Ac***, estimates of changes in capacitance (ΔC_m; ***Aa***), series resistance (ΔR_s; ***Ab***), and membrane resistance (ΔR_m; ***Ac***) after increasing the membrane capacitance of the axon terminal by 90 fF (corresponding to an increase in surface area of 10 μm^2 with specific capacitance 0.9 $\mu F\ cm^{-2}$). Estimates indicated as a function of sine wave stimulation frequency (100 Hz - 10 kHz) for two different values of R_s ($R_{s\ (theory)}$; 10 and 100 MΩ; ***A***, ***B***). Theoretical parameter value indicated by *red* horizontal lines (***Aa*** - ***Ac***, ***Ba*** - ***Bc***). The sine wave voltage stimulus amplitude was ± 15 mV (from V_{hold} = -80 mV; ***A***, ***B***). ***B***, as in ***A***, but with SEClamp connected to soma. ***Ba*** - ***Bc*** (as in ***Aa*** - ***Ac***), SEClamp connected to soma, two different values of R_s ($R_{s\ (theory)}$; 10 and 100 MΩ).

Estimates of release kinetics for the readily releasable pool

As detailed in the Discussion, the slow deactivation kinetics for the Ca^{2+} tail current in rod bipolar cells may have confounded our estimate for the release kinetics of the readily releasable pool of vesicles. Specifically, we were concerned that the slow deactivation kinetics observed experimentally do not reflect inherent properties of the ion channels themselves, but instead reflect an artifact related to the high series resistance (R_s) encountered in several terminal-end recordings. To investigate this, we performed NEURON simulations (see Methods) with the same computer model of a rod bipolar cell used for the exocytosis studies (Fig. 2, 3; for parameters, see Oltedal et al., 2009) after incorporating a Hodgkin-Huxley style model for an L-type Ca^{2+} current. Because no model has been published for L-type Ca^{2+} current in rod bipolar cells, we used the model specification of McCormick and Huguenard (1992) for thalamocortical neurons. According to this model, the Ca^{2+} current (I_{Ca}) is given by the following equation:

$$I_{Ca} = m^2 \phi_{Ca}(V) \qquad (1)$$

where m is the activation variable and $\phi_{Ca}(V)$ is the Ca^{2+} flux predicted by the Goldman-Hodgkin-Katz current equation:

$$\phi(V) = P_{Ca} z^2 \frac{VF^2}{RT} \frac{\left[Ca^{2+}\right]_i - \left[Ca^{2+}\right]_o \exp\left(-zVF/RT\right)}{1 - \exp\left(-zVF/RT\right)} \qquad (2)$$

where z is the valence (+2), P_{Ca} is the maximal Ca^{2+} permeability, $[Ca^{2+}]_i$ is the free internal Ca^{2+} concentration, $[Ca^{2+}]_o$ is the free external Ca^{2+} concentration, V is the membrane potential, F is Faraday's constant, R is the gas constant, and T is the absolute temperature. The activation variable m was described by the following

voltage-sensitive opening (α) and closing (β) rate constants for transitions between open and closed states:

$$\alpha_m(V) = \frac{1.6}{1 + \exp\left[-0.072(V - 5.0)\right]} \quad (3)$$

$$\beta_m(V) = \frac{0.02(V - 1.31)}{\exp\left[(V - 1.31)/5.36\right] - 1} \quad (4)$$

The internal concentration of free Ca^{2+} was set to 20 nM (estimated from the composition of our intracellular solution with "Patcher's Power Tools" for IGOR Pro; http://www.mpibpc.mpg.de/abteilungen/140/software/index.html) and the external concentration was set to 2.5 mM (for simplicity we assumed an activity coefficient of 1). The voltage-dependent I_{Ca} was specified as a density mechanism in NEURON and included in axon terminal endings T1+T2 or in T1+T2+T3 (Suppl. Fig. 1A). The maximal Ca^{2+} permeability was set to 2.4×10^{-4} cm s^{-1}, after adjustment to give realistic peak current amplitudes (~20 pA for a voltage step from -60 to -10 mV for I_{Ca} in T1+T2, ~30 pA for I_{Ca} in T1+T2+T3). To simulate voltage-clamp recording, we inserted an SEClamp point process at T1 and ran simulations with R_s equal to 1, 50, 100, and 200 MΩ. All simulations were run with a fixed time step of 1 μs.

To examine the effect of R_s on the activation kinetics of I_{Ca}, we applied voltage pulses from V_{hold} = -60 mV to -10 mV. After subtracting leak and capacitive currents, the activation phase was fit with a single exponential function to determine the time constant of activation (τ_{act}). As illustrated in Suppl. Fig. 2B, τ_{act} increased ~2-fold when R_s increased from 1 to 200 MΩ. When I_{Ca} was included in T3 in addition to T1 and T2, τ_{act} was slowed by an approximately fixed magnitude that was independent of R_s (Suppl. Fig. 2B).

To examine the effect of R_s on the deactivation kinetics of I_{Ca}, we applied 10-ms voltage pulses from V_{hold} = -60 mV to mV to +90 mV, followed by return to -60 mV. After subtracting leak and capacitive currents, the deactivation time constant, τ_{deact}, was determined by fitting the decay phase of the Ca^{2+} tail current with a single-exponential function. As is illustrated in Suppl. Fig. 2C, τ_{deact} increased 3- to 4-fold when R_s increased from 1 to 200 MΩ. Similar to the observation for τ_{act}, τ_{deact} was slowed by an approximately fixed magnitude, almost independent of R_s, when I_{Ca} was included in T3 in addition to T1 and T2 (Suppl. Fig. 2C). While increased R_s slowed the deactivation kinetics, it also decreased the peak amplitude of I_{Ca}, such that the time integral of the Ca^{2+} tail current (Q_{Ca}) only increased by ~30% when R_s increased from 1 to 200 MΩ (Suppl. Fig. 2D).

Qualitatively, the changes of τ_{act}, τ_{deact}, and Q_{Ca} in the simulations are consistent with the idea that high R_s in our recordings of rod bipolar cells resulted in an overestimation of τ_{deact} for the observed Ca^{2+} tail current. Consequently, the lack of adequate voltage control in the experiments with brief depolarization to +90 mV might have led to an increased influx of Ca^{2+} upon direct return of the membrane potential to -60 mV. Furthermore, the increased Ca^{2+} influx might have evoked exocytosis that would have been smaller, or not have occurred at all, with adequate voltage control. Quantitatively, however, the effect of increasing R_s on the kinetics of the simulated I_{Ca} seems to be relatively mild. Accordingly, the deactivation kinetics of I_{Ca} in rod bipolar cells seem genuinely slow and not simply a result of high R_s. If it is slowed down by the same factor observed for the simulated I_{Ca}, the true τ_{deact} might in the worst case be 1 - 2 ms, still considerably slower than ~120 μs observed for the corresponding I_{Ca} in goldfish bipolar cells (Mennerick & Matthews, 1996). Further clarification of this point

will require detailed investigation of the kinetic properties of Ca^{2+} currents in rod bipolar cells.

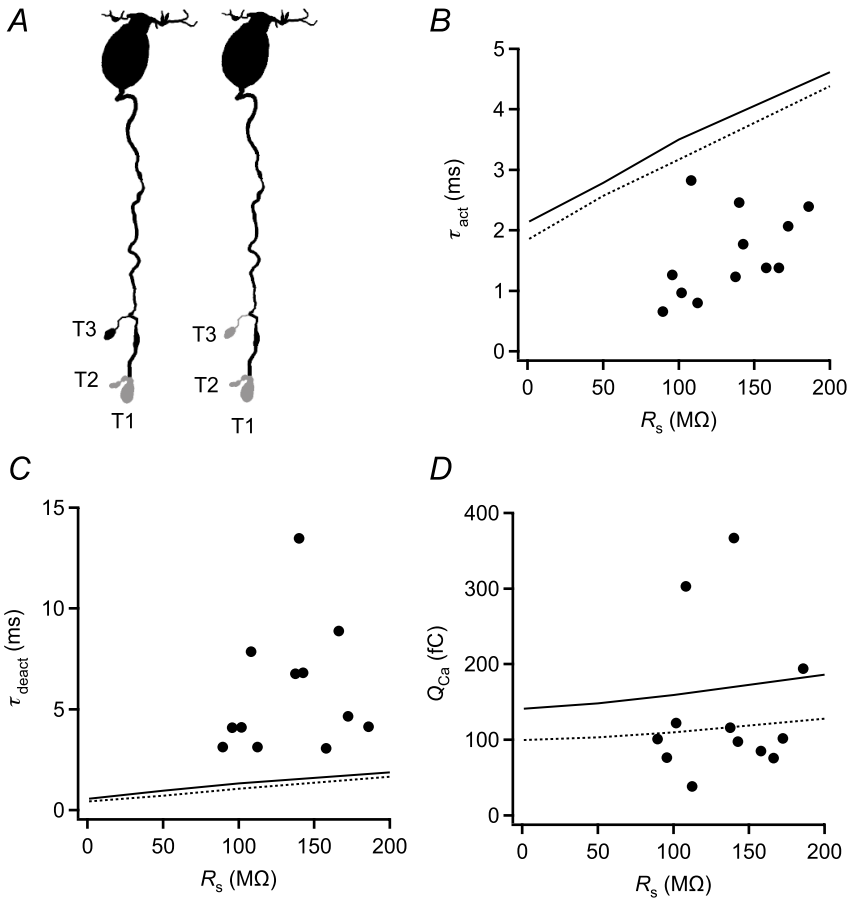

Supplementary Figure 2. Computer simulations of the influence of series resistance (R_s) on kinetics of L-type voltage-gated Ca^{2+} current in rod bipolar axon terminals. ***A***, shape plots of morphologically reconstructed rod bipolar cell used for computer simulations. A voltage-gated conductance for L-type Ca^{2+} current (see specification in text) was inserted in two (T1+T2; *gray*; *left*) or three (T1+T2+T3; *gray*; *right*) of the axonal endings. An idealized single-electrode voltage clamp (SEClamp; not shown) was connected to axonal ending T1. ***B***, activation time constant (τ_{act}) for Ca^{2+} current evoked by a voltage step from V_{hold} = -60 mV to -10 mV as a function of R_s (1, 50, 100, and 200 MΩ; SEClamp). The simulations were performed with the Ca^{2+} conductance

inserted in T1+T2 (dotted line) or T1+T2+T3 (continuous line) (***B*** - ***D***). For comparison, experimental data from real rod bipolar cells recorded with the same stimulus paradigm are included (circles; ***B*** - ***D***). ***C***, deactivation time constant (τ_{deact}) for Ca^{2+} tail current evoked by a 10-ms voltage pulse from V_{hold} = -60 to +90 mV, followed by return to -60 mV. The simulations were performed for a series of R_s values (as in ***B***). ***D***, charge integral during Ca^{2+} tail current (in ***C***) as a function of R_s.

References

McCormick DA & Huguenard JR (1992). A model of the electrophysiological properties of thalamocortical neurons. *J Neurophysiol* **68,** 1384-1400.

Mennerick S & Matthews G (1996). Ultrafast exocytosis elicited by calcium current in synaptic terminals of retinal bipolar neurons. *Neuron* **17,** 1241-1249.

Oltedal L, Mørkve SH, Veruki ML & Hartveit E (2007). Patch-clamp investigations and compartmental modeling of rod bipolar axon terminals in an in vitro thin-slice preparation of the mammalian retina. *J Neurophysiol* **97,** 1171-1187.

Oltedal L, Veruki ML & Hartveit E (2009). Passive membrane properties and electrotonic signal processing in retinal rod bipolar cells. *J Physiol* **587,** 829-849.

Wan Q-F, Vila A, Zhou Z-Y & Heidelberger R (2008). Synaptic vesicle dynamics in mouse rod bipolar cells. *Vis Neurosci* **25,** 523-533.

Zhou Z-Y, Wan Q-F, Thakur P & Heidelberger R (2006). Capacitance measurements in the mouse rod bipolar cell identify a pool of releasable synaptic vesicles. *J Neurophysiol* **96,** 2539-2548.